Case Studies in Thermal Engineering 45 (2023) 102911

Contents lists available at ScienceDirect

Case Studies in Thermal Engineering

journal homepage: www.elsevier.com/locate/csite

Prabhakar fractional simulation for inspection of CMC-based nanofluid flowing through a poured vertical channel

Ali Raza [a,b], Ahmed M. Abed [c,d], M.Y. Almusawa [e], Laila F. Seddek [f,g], Ali Hasan Ali [h,i,*]

[a] Department of Mathematics, University of Engineering and Technology Lahore, Pakistan
[b] Department of Mathematics, Minhaj University Lahore, Pakistan
[c] Department of Industrial Engineering, College of Engineering, Prince Sattam Bin Abdulaziz University, Al Kharj, 16273, Saudi Arabia
[d] Industrial Engineering Department, Zagazig University, Zagazig, 44519, Egypt
[e] Department of Mathematics, Faculty of Science, Jazan University, Jazan, 45142, Saudi Arabia
[f] Department of Mathematics, College of Science and Humanities in Al-Kharj, Prince Sattam bin Abdulaziz University, Al-Kharj P.O. Box, 11942, Saudi Arabia
[g] Department of Engineering Mathematics and Physics, Faculty of Engineering, Zagazig University, Zagazig, 44519, Egypt
[h] Institute of Mathematics, University of Debrecen, Pf. 400, H-4002, Debrecen, Hungary
[i] Department of Mathematics, College of Education for Pure Sciences, University of Basrah, Basrah, 61001, Iraq

ARTICLE INFO

Handling Editor: Huihe Qiu

Keywords:
Prabhakar fractional derivative
CMC-nanofluid
Viscous flow
Vertical channel
Porous medium

ABSTRACT

Nanofluids can be used in different solar thermal systems. Solar energy devices utilized in industries and nanofluids as a source of solar energy in thermal engineering are two other sources of solar energy, according to the article. This work inspects a viscous, incompressible nanofluid made of different (graphene oxide (GO) and molybdenum disulfide (MoS_2)) nanoparticles suspended in carboxymethyl cellulose (CMC). The governed model also considers permeability and angled magnetic effects. Due to memory effects, classical derivatives cannot explore and estimate the physical significance of several fluid limitations. We have addressed the issues with nanofluid suspension using the Prabhakar fractional derivative definition, the quickest and latest modern fractional technique. First, the governed leading equations are transferred to a fractional version using the integral transform technique and Laplace transform, and then it is resolved with various numerical approaches. Each constraint visual impact and significance are analyzed by varying their considered values. The numerical influences of the heat and flow rate are observed at multiple time values. Therefore, we deduce that the momentum and heat profiles are slowed as the Prabhakar fractional restraints increase. While with the increment in the radiation parameter, the velocity profile shows an increasing behavior. Furthermore, the impact of graphene oxide-based suspension is more significant than molybdenum disulfide nanofluid on all governed equations due to the physical features of the considered nanoparticles.

* Corresponding author. Institute of Mathematics, University of Debrecen, Pf. 400, H-4002, Debrecen, Hungary.
E-mail addresses: aliraza.math@mul.edu.pk (A. Raza), a.abed@psau.edu.sa (A.M. Abed), malmusawi@jazanu.edu.sa (M.Y. Almusawa), l.morad@psau.edu.sa (L.F. Seddek), ali.hasan@science.unideb.hu (A.H. Ali).

https://doi.org/10.1016/j.csite.2023.102911
Received 30 January 2023; Received in revised form 6 March 2023; Accepted 16 March 2023
Available online 17 March 2023

Nomenclature:

Symbol	Quantity.Unit
W_1	Fluid velocity. (m/s)
t	Times (s)
g	Gravity acceleration (m/s^2)
M	Magnetic field $(-)$
C_p	Specific heat at constant pressure (J/kgK)
k_{nf}	Nanofluids Thermal conductivity (W/mk)
μ_{nf}	Dynamic viscosity (Kg/ms)
C_f	Skin friction $(-)$
ρ_{nf}	Nanofluid density (Kg/m^3)
U_0	Characteristic velocity (ms^{-1})
θ	Inclination angle $(-)$
Gm	Mass Grashof number $(-)$
Pe	Peclet number $(-)$
T_w	Wall temperature (K)
Gr	Heat Grashof number $(-)$
T_d	Ambient temperature (K)
φ	Volume Fraction of Nanofluid $(-)$
α, β, γ	Fractional parameters $(-)$
Sc	Schmidt number $(-)$
q	Laplace transform variable $(-)$
B_o	Magnetic field strength (Kg/s^2)
β_T	Thermal expansion coefficient $(1/k)$
σ	Electrical conductivity $(-)$
Nu	Nusselt number $(-)$
Sh	Sherwood number $(-)$

1. Introduction

Nanofluids are a combination of Nano-sized particles often suspended in the base fluid to improve the thermodynamic properties of the base fluids. Researchers have shifted their focus to the use of nanoparticles, such as carbon nanotubes, oxides, metals, nitrides, or carbides, along with numerous base fluids, including water, tri-ethylene glycol, and ethylene, engine oil, kerosene, in order to increase the exterior area and thermal expansion of typical fluids. There is no getting around the reality that typical fluids have low thermal conductivities and that these thermal conductivities can be increased by combining 1% of dispersed nanoparticles from 40 to 150%. At least two materials with different physical and chemical properties, like heat flow and thermal conductivity, were mixed to create this new product. In essence, this new substance has undergone an excessive transformation due to a hybrid nanofluid. The performance of thermal solid conductivity in nanofluids attracted the attention of many researchers. Choi [1] first proposed the term "nanofluid" and determined that the features of heat transmission in ordinary fluids might be amended by suspending nanoparticles. Subsequently, Buongiorno et al. [2] proposed a model that predicts the amplification of heat transmission by nanofluids due to the Brownian diffusion of nanomaterials. On the MHD free convection heat transmission supplied with Al_2O_3-water nanofluid, Sheikh et al. [3] examined the impact of Brownian motion and thermosiphon-physical factors. They applied the control volume-based finite element method to the leading equations. They concluded that the buoyancy ratio value is an essential determinant of the Nusselt number, whereas the Lewis and Hartmann numbers are decreasing functions. The non-Newtonian copper-water nanofluid with free convection was seen by Domairry et al. [4] between two infinitely parallel vertical flat surfaces. The leading model was transformed into ODE using the differential modeling approach. They noticed that when the volume percentage of nanoparticles grew, the thermal boundary layer's thickness decreased while the velocity boundary layer's thickness increased.

One of the first to demonstrate nanofluids with nano-particles was Choi in 1995. There are many advantages that nanofluids can offer, including thermal conductivity. Choi and Eastman [1] designed most of these for use in fluid mechanics, mechanical design, and biomedical engineering. The research of Ali et al. [5] on the sporadic scientific evidence of hybrid nanofluids and its applications in mass and heat transmission was published. Examples of Casson nanofluid complementary convection flow settings over an unending vertical panel were presented by Ahmad et al. [6] in their study. The flow of a hybrid nanofluid via the cone-shaped aperture was studied by Gul et al. [7]. Rafique et al. [8] defined the Casson nanofluid flow with mass and energy transport on an inclined slanted surface. Using a hybrid fractional operator, Asjad et al. [9] studied the thermo-physical properties of clay nanofluids. Ikram et al. [10] used a constant proportional Caputo fractional operator to build the fractional model of a Brinkman-Type Fluid transporting Hybrid Nano-particles in a confined microchannel. Other recent work on the nanofluid can be seen in Refs. [11–15].

Several researchers [16–20] have studied the viscid fluid flowing among vertical side walls to the bottom plate over which the fluid flows. Although the fluid velocity in these open channel flows varies at every location, the calculations used to determine the fluid's velocity depend entirely on the flow rate in the channel's center. The side walls effects on the fluid's motion are significant and strongly correlated with time since they intensify with elapsed time. In the absence of side walls, Vieru et al. [21] investigated the solutions to a fractional Maxwell fluid model. Wang et al. [22] have utilized the recent definition of the fractional technique to explore the impacts of different constraints on the sediment suspension in ice-covered channels. In Ref. [23] khan et al. have used the CF-fractional derivative definition to explore the physical significance of fractional Brinkman-type nanofluid flowing in a closed channel. Using MHD and porosity, Rao et al. [24] discovered the accurate Casson fluid solution close to an infinite, exponentially accelerating, and vertical channel. The heat transport combined with graphene oxide nanoparticles was examined by Aman et al. [25] using the CG fractional derivatives. Goud et al. [26] used the finite element method to precisely solve the Casson fluid natural convection MHD flow near a vertical plate via a porous material. The behavior of a non-Newtonian micro-polar Casson fluid pulsatile flow in a restricted channel under the influence of the Lorentz force is investigated by Ali et al. [27]. Using the use of fractional derivatives, Sunthrayuth et al. [28] investigate the fractional Casson fluid flow solution over a porous channel. They have utilized the CF-fractional derivative and examined the effect of porosity at the boundaries of the oscillating channel.

Many industrial environments use channel flow, comprising thermal exchangers in the power plants industry. While many natural two-phase systems work Newtonianally, there are many related submissions where the continuous liquid phase reveals non-Newtonian flow features. Many instances exist in the biochemical, biomedical, and food processing industries [29]. In a channel, Zheng. et al. [30] looked at how constructing a vortex generator affected the flow of fluids and the heat evolution of hybrid nanofluids. In all research areas, fractional calculus has recently been used as a tool. Non-integer derivatives are preferred over classical calculus in any scientific investigation. Applications of fractional order calculus have been cited in medicine, viscoelasticity, diffusion, wavelets, electrochemistry, fractional filters, combustion, geophysics, fractional, and numerous other branches of science and technology [31]. Compared to solutions produced from analogous integer order differential equations, non-integer order differential equations are shown to approximate real-world conditions more closely. Numerous fluid dynamics studies have shown that various fractional operators help understand heat and mass transport processes. According to Shah et al. [32] examination of the electro-osmotic flow of Oldroyd-B fluid in a micro-channel, the fluid velocity exhibits a dual behavior for both vast and slight values of time when it is subject to the Caputo-Fabrizio fractional parameter. More work on the channel flow can be seen in Refs. [33–38].

Because academics are curious, many characterization techniques of fractional derivatives have been published in the literature. To solve the issues with past research on the singularity problem of the kernel, Caputo-Fabrizio (CF) developed a fractional order derivative predicated on an exponential function. In recent years, modeling most dynamic processes typically involving memory factors has heavily relied on fractional derivatives (FDs) and fractional differential equations. Typically, global fractional derivatives can be used to solve dynamic models, including the full memory effect. In contrast, only fractional derivatives with short memories can be

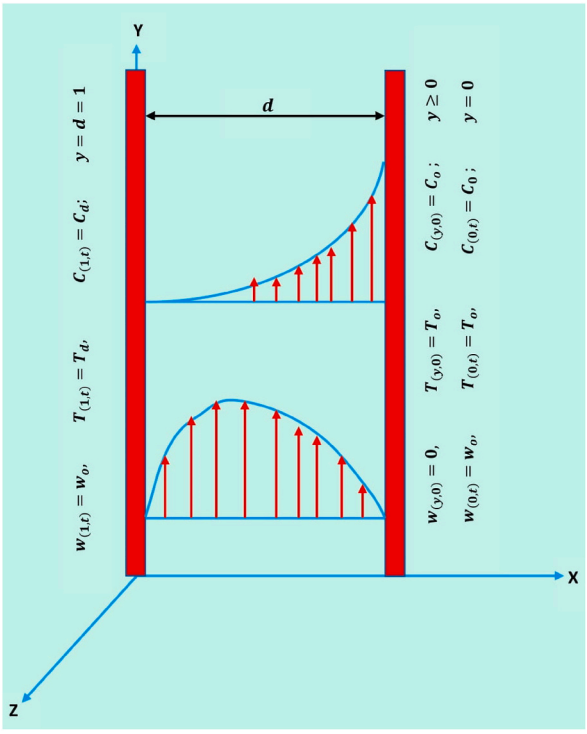

Fig. 1. Flow geometry.

used to solve models involving the local memory effect. There is no distinct kernel in the Caputo and Fabrizio fractional model [39]. Recent works in fractional calculus have given this concept of fractional order a lot of thought. Multiple researchers have adopted the definition of CF for numerous scientific investigations due to its ubiquitous use. Atangana and Nieto et al. [40] developed a novel formulation to solve the problem of the kernel's non-locality in the definition of CF. Atangana [41] provided the most recent explanation of fractional derivatives without these issues. The term "AB derivatives" is new and is infrequently used in the study. This most modern idea of AB fractional derivatives was employed by Arif et al. [42], and the current problem is also applied to CF fractional derivatives in order to compare the two concepts. Another well-pair stress fluid model is also solved in this paper using a closed-form channel and an external pressure gradient despite using the fractional Caputo and CF models. Akhtar et al. [43] estimated closed-form solutions for channels (CSF). You may see other examples of fractional derivatives being used to solve various fluid issues in Refs. [5, 14,44–46].

Based on past research, this study examines a nanofluid consisting of carboxymethyl cellulose (CMC) as a base fluid with a variety of graphene oxide (GO) and molybdenum disulfide (MoS_2) nanoparticles. To close this knowledge gap, PDEs are used to develop the guided model for the suggested flow system. Because when memory effects are present, classical derivatives cannot evaluate and assess the physical trend of many flow limits. Generalized Fourier, Fick's law, and the leading and most recent fractional technique, the Prabhakar fractional derivative, are used to addressing the problem. The LT method is used to solve the dimensionless classical model after it has been transformed into a non-integer ordered model. The visual inspection looks at how significant physical and frictional properties behave and how they affect things. As a result, GO-based nanofluid has a more significant impact on the governed model than MoS_2-based nanofluid due to the physical significance of considered nanoparticles.

2. Problem description

Consider the flow of a graphene and molybdenum-disulfide-containing carboxymethyl cellulose-based nanofluid in a vertical channel under an unsteady, free convective, and incompressible condition. Fluid moves in the x-direction while the y-axis is adjusted to be orthogonal to the flow direction. The flow with an inclination of angle θ direction is subjected to a continuous magnetic field of strength B_0 (along x -axis). The system is at rest at time $t = 0$, but as time passes, the static fluid starts to flow due to changes in the temperature field and oscillations of the static plates, as depicted in Fig. 1. After $t > 0$, the temperature of the channel increases from T_0 to T_w, increasing the buoyancy force and causing the fluid to flow in the x-direction. The effect of viscous dissipation is neglected in the energy equation. The temperatures of the left and right plates are represented by T_0 and T_d in the vertical channel, respectively, while the concentrations of the left and right plates are denoted by C_0 and C_d. The following presumptions are made in relation to this flow model.

- The length of parallel plates is infinite at width d.
- The x-axis is aligned with the oscillating plates, which are vertical to the y-axis.
- The hybrid nanofluid is moving perpendicular to the y-axis and in the x-direction.
- At time $t \leq 0$, the temperature and concentration, T_o and C_o, respectively, have constant values.
- The boundary of the vertical channel is also considered while analyzing the influence of the porosity parameter.
- The x-direction is accelerated by various hybrid nanofluids made up of mixed nanoparticles.
- The momentum equation disregards the effect of viscous dissipation.
- A magnetic field with a constant B_o field intensity is present around the flowing fluid.

By utilizing the Boussinseq's approximation [47] and Roseland approximations [48], the governed partial differential equations can be formulated as follows [25].

$$\rho_{nf}\frac{\partial w_1(y,t)}{\partial t} = \mu_{nf}\frac{\partial^2 w_1(y,t)}{\partial y^2} + g(\rho\beta_T)_{nf}(T_1(y,t) - T_o) - \left(\sigma_{nf}B_o^2\, sin(\theta) + \frac{\mu_{nf}\varphi}{k_1}\right)w_1(y,t) + g(\rho\beta_c)_{nf}(C_1(y,t) - C_o) \tag{1}$$

$$\left(\rho C_p\right)_{nf}\frac{\partial T_1(y,t)}{\partial t} = -\frac{\partial \delta_1(y,t)}{\partial y} + 4\alpha_o^2(T - T_o), \delta_1(y,t) = -k_{nf}\frac{\partial T_1(y,t)}{\partial y} \tag{2}$$

$$\frac{\partial C_1(y,t)}{\partial t} = -\frac{\partial J_1(y,t)}{\partial y}, J_1(y,t) = -D_{nf}\frac{\partial C_1(y,t)}{\partial y} \tag{3}$$

Here, $\frac{\partial q_r}{\partial y} = 4\alpha_o^2(T - T_o)$ is used to indicate the radiative heat flux, $\delta_1(y,t)$ and $J_1(y,t)$ indicates the Fourier and Fick's laws considered in thermal and concentration profiles. Where φ is the nanoparticles volume fraction, ρ_s and ρ_f is the density of the graphene nanoparticles and base fluid, β_s, β_f , $(\rho C_p)_s$, $(\rho C_p)_f$, K_s, K_s , are the volumetric coefficient of thermal expansion, specific heat capacities, and thermal conductivities of nanoparticles and CMC-base fluid, respectively, with the succeeding boundary conditions

$$w_1(y,0) = 0, T_1(y,0) = T_o, C_1(y,0) = C_o \tag{4}$$

$$w_1(0,t) = w_o, T_1(0,t) = T_o, C_1(0,t) = C_0 \tag{5}$$

$$w_1(d,t) = w_o, T_1(d,t) = T_d, C_1(d,t) = C_d \tag{6}$$

The initial condition for governed equations is taken into account at $t = 0$ in condition (4) above, and condition (5) represents the boundary condition at $y = 0$, indicating the static position of the hybrid nanofluid for $y = 0$. In the contrary, condition (6) displays the motions of the fluid's flow at y = d. And the non-dimensional constraints

$$y^* = \frac{y}{d}, w_1^* = \frac{w_1}{U_o}, t^* = \frac{U_o^2}{\upsilon_f} t, T_1^* = \frac{T_1 - T_o}{T_d - T_o} = \frac{T_1 - T_o}{\Delta T}$$

$$C_1^* = \frac{C_1 - C_o}{C_d - C_o} = \frac{C_1 - C_o}{\Delta C}, \delta_1^* = \frac{\delta_1}{\delta_o}, J_1^* = \frac{J_1}{J_o}$$

ignoring the steric notation and substituting the governing equations and conditions (1) through (6). The following are the non-dimensional governed equations that we obtain

$$\mathrm{a}_1 Re \frac{\partial w_1(y,t)}{\partial t} = \mathrm{a}_2 \frac{\partial^2 w_1(y,t)}{\partial y^2} - \left(M\, sin(\theta) + \frac{\mathrm{a}_2}{K}\right) w_1(y,t) + \mathrm{a}_3 Gr T_1(y,t) + \mathrm{a}_4 Gm\, C_1(y,t) \tag{7}$$

$$Pe\, \frac{\partial T_1(y,t)}{\partial t} = -\frac{\partial \delta_1(y,t)}{\partial y} + N^2 T_1(y,t)\, \delta_1(y,t) = -\frac{\partial T_1(y,t)}{\partial y} \tag{8}$$

$$b_3 \frac{\partial C_1(y,t)}{\partial t} = -\frac{\partial J_1(y,t)}{\partial y}, J_1(y,t) = -\frac{\partial C_1(y,t)}{\partial y} \tag{9}$$

and the succeeding dimensionless conditions

$$w_1(y,0) = 0, T_1(y,0) = 0, T_1(y,0) = 0 \tag{10}$$

$$w_1(0,t) = 0, T_1(0,t) = 0, C_1(0,t) = 0 \tag{11}$$

$$w_1(1,t) = 0, T_1(1,t) = 1, C_1(1,t) = 1 \tag{12}$$

Where:

$$Re = \frac{U_o d}{\nu}, M = \frac{\sigma_f B_o^2 d^2}{\mu}, K = \frac{k_1}{d}, N^2 = \frac{4\alpha_o^2 d^2}{k_f}$$

$$Pr = \frac{\left(\mu C_p\right)_f}{\kappa_f}, Gr = \frac{g(\beta_T)_f d^2 (T_d - T_o)}{\nu U_o}, Sc = \frac{\upsilon_f}{D}, Gm = \frac{g(\beta_c)_f d^2 \Delta C}{\nu U_o}$$

are the Reynolds number, magnetic, Porosity, radiation, Prandtl number, heat grashoof number, Schmidt number, and mass grashoof number, respectively.

Basic definitions:

The single-parametric Mittage-Leffler function

$$E_\alpha(z) = \sum_{n=0}^{\infty} \frac{z^n}{\Gamma(\alpha n + 1)}$$

This has been looked into by Mittage-Leffler [50]. After a while, Wiman [51] studied the double-parametric Mittage-Leffler functions, which are a more extensive version of the single-parametric function.

$$E_{\alpha,\beta}(f) = \sum_{i=0}^{\infty} \frac{f^i}{\Gamma(\alpha i + \beta)} \tag{13}$$

In [52], the authors presented the triple-parametric Mittage-Leffler function

$$E_{\alpha,\beta}^{\gamma}(f) = \sum_{i=0}^{\infty} \frac{(\gamma)_i f^i}{\mathrm{i!}\, \Gamma(\alpha i + \beta)}$$

with

$$E_\alpha(f) = E_{\alpha,1}^1(f), E_{\alpha,\beta}(f) = E_{\alpha,\beta}^{\gamma}(f), E_{1,1}^1(f) = \exp(f)$$

$$\mathscr{L}\left\{t^{\beta-1} E_{\alpha,\beta}^{-\gamma}(\alpha t^\alpha)\right\} = q^{-\beta}(1 - \alpha q^{-\alpha})^{\gamma} \tag{14}$$

(Prabhakar kernel):

$$e^{\gamma}_{\alpha,\beta}(\alpha;t)=t^{\beta-1}E^{\gamma}_{\alpha,\beta}(\alpha t^{\alpha});\quad t\in\mathscr{R}$$

is the mathematical interpolation of the Prabhakar kernel.

(Prabhakar Integral) This can be stated as [53,54].

$$E^{\gamma}_{\alpha,\beta,\alpha}f(t)=e^{\gamma}_{\alpha,\beta}(\alpha;t)*h(t)=\int_0^t(t-x)^{\beta-1}E^{\gamma}_{\alpha,\beta}(\alpha(t-x)^{\alpha})h(x)dx$$

with its Laplace

$$\mathscr{L}\left\{E^{\gamma}_{\alpha,\beta,\alpha}h(t)\right\}(s)=\mathscr{L}\left\{e^{\gamma}_{\alpha,\beta}(\alpha;t)\right\}\mathscr{L}\{h(t)\}=\frac{s^{\alpha\gamma-\beta}}{(s^{\alpha}-\alpha)^{\gamma}}\mathscr{L}\{h(t)\} \tag{15}$$

The mathematical notation of regularized Prabhakar is specified as [53,54].

$${}^{C}\mathfrak{D}^{\gamma}_{\alpha,\beta,\alpha}g(t)=E^{-\gamma}_{\alpha,m-\beta,\alpha}g^{m}(t)=e^{-\gamma}_{\alpha,m-\beta}(\alpha;t)*g^{m}(t)$$

$$=\int_0^t(t-x)^{m-\beta-1}E^{-\gamma}_{\alpha,m-\beta}(\alpha(t-x)^{\alpha})g^{m}(x)d(x) \tag{16}$$

$$\mathscr{L}\left[{}^{C}\mathfrak{D}^{\gamma}_{\alpha,\beta,\alpha}\,\mathrm{f}(t)\right]=\mathscr{L}\left[f^{n}(t)*e^{-\gamma}_{\alpha,n-\beta}(\alpha;t)\right]=\mathscr{L}\{f^{n}(t)\}\mathscr{L}\left\{e^{-\gamma}_{\alpha,n-\beta}(\alpha;t)\right\}$$

$$=\mathscr{L}\{f^{n}(t)\}s^{\beta-m}(1-\alpha s^{-\alpha})^{\gamma} \tag{17}$$

By assuming $\beta=\gamma=0$, we might be able to achieve the standard Fourier's rule. Given that Fourier's law efficiently describes the Prabhakar fractional derivative, the subsequent Fick's and Fourier's laws likewise apply to the Prabhakar derivative.

$$\delta_1(y,t)=-{}^{C}\mathfrak{D}^{-\gamma}_{\alpha,\beta,\alpha}\frac{\partial T_1(y,t)}{\partial y} \tag{18}$$

$$J_1(y,t)=-{}^{C}\mathfrak{D}^{-\gamma}_{\alpha,\beta,\alpha}\frac{\partial C_1(y,t)}{\partial y} \tag{19}$$

3. Solution of the model

3.1. Thermal field

For the simulations of heat equation taking the LT on Eqs. (8) and (18) as follows

$$Pe\,q\,\overline{T}_1(y,q)=-\frac{\partial\overline{\delta}_1(y,q)}{\partial y}-N^2\overline{T}_1(y,q) \tag{20}$$

$$\overline{\delta}_1(y,q)=-q^{\beta}(1-\alpha q^{-\alpha})^{\gamma}\frac{\partial\overline{T}_1(y,q)}{\partial y} \tag{21}$$

$$\overline{T}_1(0,q)=0,\overline{T}_1(1,q)=\frac{1}{q} \tag{22}$$

Putting Eq. (21) into Eq. (20)

$$\frac{d^2\overline{T}_1(y,q)}{dy^2}-\frac{Peq-N^2}{q^{\beta}(1-\alpha q^{-\alpha})^{\gamma}}\overline{T}_1(y,q)=0 \tag{23}$$

The heat flux solution will be determined by utilizing the preceding conditions as follows

Table 1
Representation of the thermophysical properties of NFs quantities [49].

Quantities	Nanofluid Parameters
Density	$\rho_{nf}=(1-\varphi)\rho_f+\varphi\rho_s$
Dynamic Viscosity	$\mu_{nf}=\mu_f/(1-\varphi)^{5/2}$
Electrical conductivity	$\sigma_{nf}/\sigma_f=1+3(\sigma_s/\sigma_f-1)\varphi/(\sigma_s/\sigma_f+2)-(\sigma_s/\sigma_f-1)\varphi$
Thermal conductivity	$K_{nf}/K_f=k_s+2k_f-2\varphi\,(k_s-k_f)/k_s+2k_f+\varphi(k_s-k_f)$
Heat capacitance	$(\rho C_p)_{nf}=(1-\varphi)(\rho C_p)_f+\varphi(\rho C_p)_s$
Thermal Expansion Coefficient	$(\rho B_T)_{nf}=(1-\varphi)(\rho B_T)_f+\varphi(\rho B_T)_s$

Table 2
The thermal characteristics of considered nanofluid [45].

Material	*CMC*	MOS_2	*GO*
$\rho(kg/m^3)$	997	5060	1800
$C_p(J/kg\,K)$	4179	397.20	717
$k(W/m\,K)$	0.613	904.4	5000
$\beta_T(K^{-1})$	70×10^{-5}	2.842×10^{-5}	2.84×10^{-4}

$$\overline{T}_1(y,q)=\frac{1}{q}\,\frac{\mathrm{Sinh}\left[y\sqrt{\frac{\mathrm{Peq}-N^2}{q^{\beta}(1-\alpha q^{-\alpha})^{\gamma}}}\right]}{\mathrm{Sinh}\left[\sqrt{\frac{\mathrm{Peq}-N^2}{q^{\beta}(1-\alpha q^{-\alpha})^{\gamma}}}\right]} \tag{24}$$

We will utilize numerical approaches to find the inverse of Laplace's equation (24), such as Stehfest and Tzou's systems in Tables 3 and 4.

3.2. Concentration field

Like the energy equation, implementing the LT on the governed Eqs. (9) and (19).

$$b_3\,q\,\overline{C}_1(y,q)=-\frac{\partial\overline{J}_1(y,q)}{\partial y} \tag{25}$$

$$\overline{J}_1(y,q)=-q^{\beta}(1-\alpha q^{-\alpha})^{\gamma}\frac{\partial\overline{C}_1(y,q)}{\partial y} \tag{26}$$

$$\overline{C}_1(0,q)=0,\overline{C}_1(1,q)=\frac{1}{q} \tag{27}$$

Presenting Eq. (26) into (27)

$$\frac{d^2\overline{C}_1(y,q)}{dy^2}-\frac{b_3\,q^{1-\beta}}{(1-\alpha q^{-\alpha})^{\gamma}}\overline{C}_1(y,q)=0 \tag{28}$$

The solution of the concentration field will take on the following form when the above condition is used

$$\overline{C}_1(y,q)=\frac{1}{q}\,\frac{\mathrm{Sinh}\left[y\sqrt{\frac{b_3\,q^{1-\beta}}{(1-\alpha q^{-\alpha})^{\gamma}}}\right]}{\mathrm{Sinh}\left[\sqrt{\frac{b_3\,q^{1-\beta}}{(1-\alpha q^{-\alpha})^{\gamma}}}\right]} \tag{29}$$

For the inverse of Laplace's equation (23), Tables 3 and 4 will once more use numerical methods like Stehfest and Tzou's schemes.

3.3. Momentum field

This section will also employ the strategy used to resolve the momentum equation for the energy and concentration profiles. Using the LT technique and the proper conditions in Eq. (7), we obtain

$$\frac{\partial^2\overline{w}_1(y,q)}{\partial y^2}-\frac{1}{a_2}\left(M\,sin(\theta)+\frac{a_2}{K}+a_1Re\,q\right)\overline{w}_1(y,q)=-\frac{a_3\,Gr}{a_2}\,\frac{\mathrm{Sinh}\left[y\sqrt{\frac{Pe\,q-N^2}{q^{\beta}(1-\alpha q^{-\alpha})^{\gamma}}}\right]}{\mathrm{Sinh}\left[\sqrt{\frac{Pe\,q-N^2}{q^{\beta}(1-\alpha q^{-\alpha})^{\gamma}}}\right]}-\frac{a_4\,Gm}{a_2}\,\frac{\mathrm{Sinh}\left[y\sqrt{\frac{b_3\,q^{1-\beta}}{(1-\alpha q^{-\alpha})^{\gamma}}}\right]}{\mathrm{Sinh}\left[\sqrt{\frac{b_3\,q^{1-\beta}}{(1-\alpha q^{-\alpha})^{\gamma}}}\right]} \tag{30}$$

$$\overline{w}_1(0,q)=0,\overline{w}_1(1,q)=0$$

Using the above conditions, we yield

$$\begin{aligned}\overline{w}_1(y,q)=&\left(\frac{a_3Gr}{a_2q}\,\frac{1}{\left(\frac{Peq-N^2}{q^{\beta}(1-\alpha q^{-\alpha})^{\gamma}}\right)-\frac{1}{a_2}\left(Msin(\theta)+\frac{a_2}{K}+a_1Req\right)}+\frac{a_4Gm}{a_2q}\,\frac{1}{\left(\frac{b_3q^{1-\beta}}{(1-\alpha q^{-\alpha})^{\gamma}}\right)-\frac{1}{a_2}\left(Msin(\theta)+\frac{a_2}{K}+a_1Req\right)}\right)\\&\frac{\mathrm{Sinh}\left[y\sqrt{\frac{1}{a_2}\left(Msin(\theta)+\frac{a_2}{K}+a_1Req\right)}\right]}{\mathrm{Sinh}\left[\sqrt{\frac{1}{a_2}\left(Msin(\theta)+\frac{a_2}{K}+a_1Req\right)}\right]}-\frac{a_3Gr}{a_2q}\,\frac{1}{\left(\frac{Peq-N^2}{q^{\beta}(1-\alpha q^{-\alpha})^{\gamma}}\right)-\frac{1}{a_2}\left(Msin(\theta)+\frac{a_2}{K}+a_1Req\right)}\,\frac{\mathrm{Sinh}\left[y\sqrt{\frac{Peq-N^2}{q^{\beta}(1-\alpha q^{-\alpha})^{\gamma}}}\right]}{\mathrm{Sinh}\left[\sqrt{\frac{Peq-N^2}{q^{\beta}(1-\alpha q^{-\alpha})^{\gamma}}}\right]}\\&-\frac{a_4Gm}{a_2q}\,\frac{1}{\left(\frac{b_3q^{1-\beta}}{(1-\alpha q^{-\alpha})^{\gamma}}\right)-\frac{1}{a_2}\left(Msin(\theta)+\frac{a_2}{K}+a_1Req\right)}\,\frac{\mathrm{Sinh}\left[y\sqrt{\frac{b_3q^{1-\beta}}{(1-\alpha q^{-\alpha})^{\gamma}}}\right]}{\mathrm{Sinh}\left[\sqrt{\frac{b_3q^{1-\beta}}{(1-\alpha q^{-\alpha})^{\gamma}}}\right]}\end{aligned} \tag{31}$$

Table 3
The inspection of temperature, concentration and velocity profile by numerical approaches.

y	$T_{(y,t)}$ with Stehfest	$T_{(y,t)}$ with Tzou's	$C_{(y,t)}$ with Stehfest	$C_{(y,t)}$ with Tzou's	$w_{(y,t)}$ with Stehfest	$w_{(y,t)}$ with Tzou's
0.1	0.0479	0.0483	0.0707	0.0715	0.0922	0.0937
0.2	0.0985	0.0991	0.1432	0.1447	0.1780	0.1810
0.3	0.1542	0.1553	0.2191	0.2215	0.2515	0.2555
0.4	0.2185	0.2197	0.3002	0.3029	0.3065	0.3114
0.5	0.2943	0.2957	0.3885	0.3916	0.3379	0.3431
0.6	0.3857	0.3872	0.4859	0.4890	0.3409	0.3458
0.7	0.4972	0.4986	0.5943	0.5973	0.3113	0.3156
0.8	0.6339	0.6351	0.7156	0.7180	0.2460	0.2492
0.9	0.8007	0.8014	0.8510	0.8523	0.1427	0.1440

Table 4
The inspection of governed results at different time values.

y	$T_{(y,t)}$ for t = 0.5	$T_{(y,t)}$ for t = 1.0	$C_{(y,t)}$ for t = 0.5	$C_{(y,t)}$ for t = 1.0	$w_{(y,t)}$ for t = 0.5	$w_{(y,t)}$ for t = 1.0
0.1	0.0402	0.0469	0.0658	0.0768	0.0489	0.1504
0.2	0.0833	0.0966	0.1335	0.1550	0.0952	0.2894
0.3	0.1323	0.1516	0.2052	0.2360	0.1365	0.4059
0.4	0.1906	0.2150	0.2830	0.3211	0.1697	0.4901
0.5	0.2620	0.2903	0.3689	0.4120	0.1920	0.5334
0.6	0.3511	0.3814	0.4655	0.5100	0.1998	0.5294
0.7	0.4635	0.4931	0.5752	0.6166	0.1893	0.4741
0.8	0.6055	0.6305	0.7001	0.7332	0.1559	0.3659
0.9	0.7835	0.7987	0.8419	0.8608	0.0947	0.2064

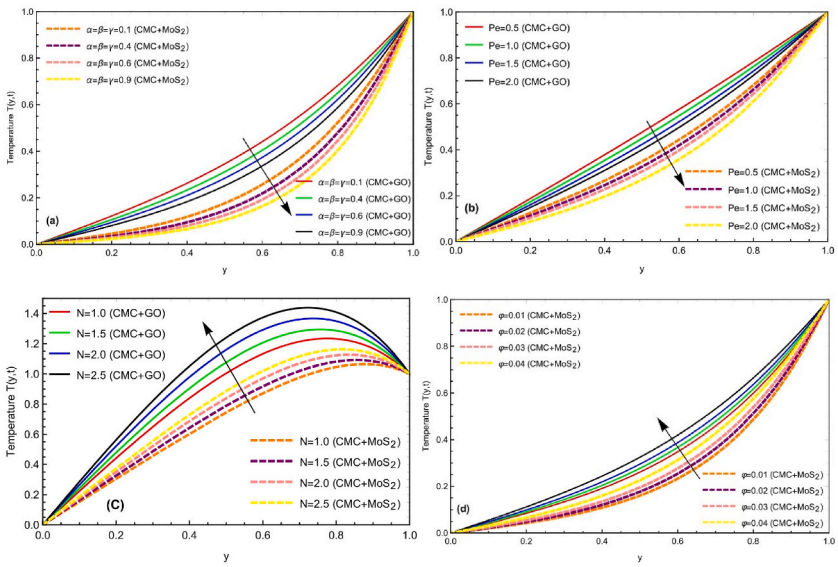

Fig. 2. Impact of different constraints on temperature field.

To examine the Laplace inverse, numerous researchers have considered altered numerical approaches. We have used the Stehfest technique to assess the thermal and momentum fields numerically. The Gaver-Stehfest method [55] is described mathematically as

$$h(y,t) = \frac{ln(2)}{t} \sum_{i=1}^{N} w_i \, \overline{h}\left(y, i\frac{ln(2)}{t}\right)$$

$$w_i = (-1)^{i+\frac{N}{2}} \sum_{s=\left[\frac{p+1}{2}\right]}^{min\left(p,\frac{N}{2}\right)} \frac{s^{\frac{N}{2}}\,(2s)!}{\left(\frac{N}{2}-s\right)!s!\,(s-1)!\,(p-s)!\,(2s-q)!}$$

We have also utilized Tzou's approach, an alternative approximation for the composition of the thermal and momentum fields, to confirm our Stehfest technique-achieved calculated values. Tzou's strategy may be described as mathematical.

$$h(y,t) = \frac{e^{4.7}}{t}\left[\frac{1}{2}\overline{h}\left(s,\frac{4.7}{t}\right) + Re\left\{\sum_{k=1}^{N}(-1)^k\,\overline{h}\left(s,\frac{4.7+k\pi i}{t}\right)\right\}\right]$$

Nusselt number, Sherwood number, and Skin friction

$$Nu = -\left.\frac{\partial T_{(y,t)}}{\partial y}\right|_{y=0} = -\mathscr{L}^{-1}\left\{\frac{\partial \overline{T}_{(0,q)}}{\partial y}\right\}$$

$$Sh = -\left.\frac{\partial C_{(y,t)}}{\partial y}\right|_{y=0} = -\mathscr{L}^{-1}\left\{\frac{\partial \overline{C}_{(0,q)}}{\partial y}\right\}$$

$$C_f = -\left.\frac{\partial w_{(y,t)}}{\partial y}\right|_{y=0} = -\mathscr{L}^{-1}\left\{\frac{\partial \overline{w}_{(0,q)}}{\partial y}\right\}$$

4. Results with discussion

In a proper channel in a porous medium, the effects of MHD mixed convection flow of graphene oxide and molybdenum disulfide nanofluid with sodium carboxymethyl cellulose as base fluid are briefly examined. Practically practical solutions for temperature, concentration, velocity field, and Nusselt number are obtained. Changing some constraints while holding others constant demonstrates how nanofluid behaves when a physical process changes. Table 1 enlists the thermophysical features of the base fluid and nanoparticles. Using Figs. 2–6, it is possible to see how different factors affect the fractional nanofluid's flow, temperature, and concentration (see Table 2).

Fig. 2 (a, b) depicts the influence of fractional constraint and the impact of Peclet number on the thermal profile by taking other constraints as constant. This can be seen that with the enhancement of fractional constraints and *Pe* number, the thermal field indicates

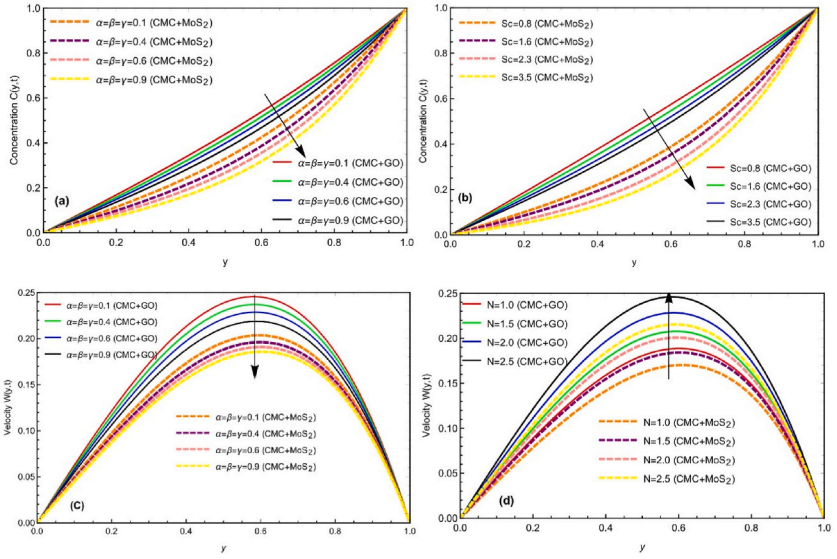

Fig. 3. Impact of $\alpha, \beta, \gamma, Sc, N$ on concentration and velocity fields with$Pe = 2.0, M = 2.57, Gr = 2.0, \mathrm{Gm} = 1.6 \quad \theta = \frac{\pi}{3}, K = 1.2, t = 1.0, \varphi = 0.02$.

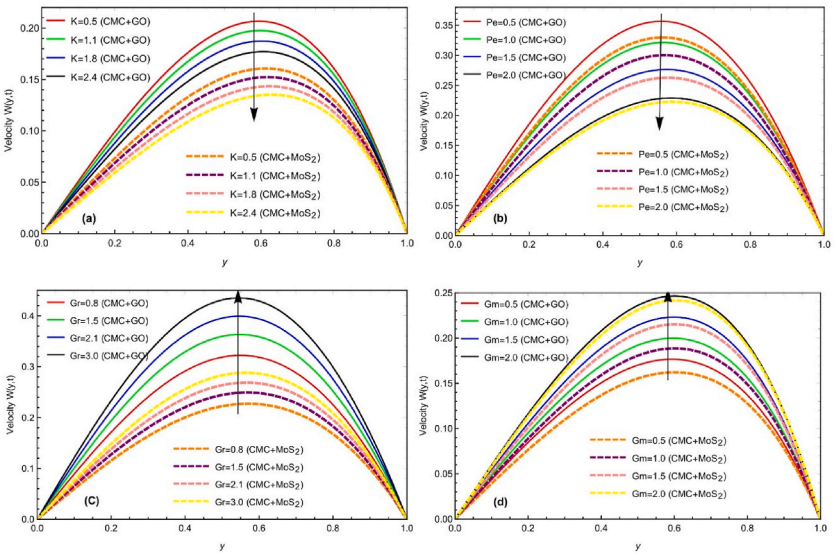

Fig. 4. Impact of K, Pe, Gr, Gm on velocity field with$\alpha, \beta, \gamma = 0.8, M = 2.57, Sc = 2.6, \mathrm{N} = 2.0, \theta = \frac{\pi}{3}, t = 1.0, \varphi = 0.02$.

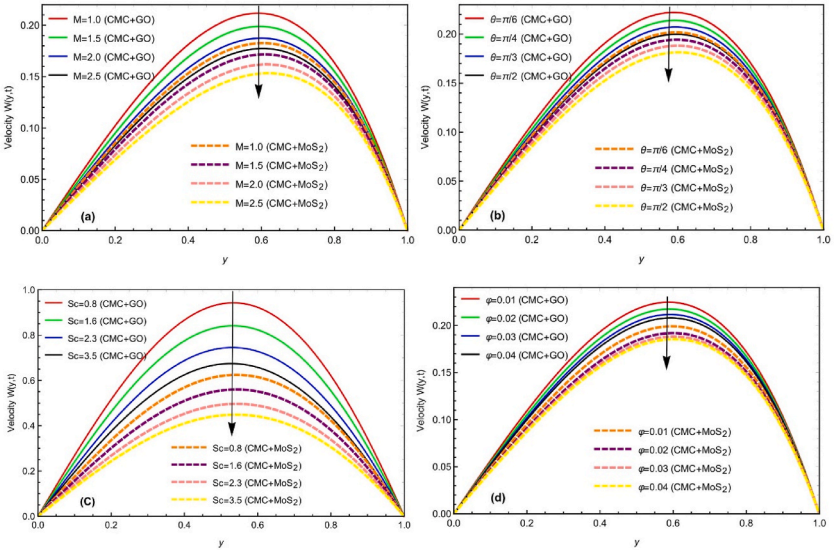

Fig. 5. Impact of M, θ, Sc, φ on velocity field with$\alpha, \beta, \gamma = 0.8, Pe = 2.0, Gr = 2.0, \mathrm{N} = 2.0, \mathrm{Gm} = 1.6, K = 1.2, t = 1.0$.

the decreasing behavior due to escalation in the thickness of the boundary layer. This is because the temperature, concentration, and momentum profiles fall when the boundary layer widens. Generally speaking, we may state that in fluid dynamics, a fractional method is preferable for adjusting the fluid characteristics' boundary layer thickness. Furthermore, this can also be analyzed for the comparison of different nanofluid that graphene oxide $(GO-CMC)$ based nanofluid has more significance on temperature field as compared to molybdenum disulfide (MoS_2-CMC) mixed nanofluid due to the physical characteristics of the considered nanofluid. It is evident that GO-based nanofluid has a greater temperature than MoS_2-based nanofluid. Physically, GO-based nanofluid warms up more quickly than those made of other nanoparticles because GO-based nanofluid's viscosity and Prandtl values are much lower. Fig. 2 (c, d) shows the visual impacts of radiation parameter N and volume fractionφ on the temperature field, respectively. Due to the increase in radiation parameters enhances the heat energy transfer, resulting in the temperature field. While holding all other parameters fixed, Fig. 2 shows that temperature rises as volume fraction rises for both fractional and regular nanofluid. Physically, the fluid becomes hotter by boosting the volume fraction of nanoparticles in the base fluid, which improves thermal conductivity. The physical influence of fractional constraints and Schmidt number on the concentration field are analyzed in Fig. 3 (a, b) on the concentration of flowing fluid. Again like the thermal field, the concentration field decelerates with the improvement in fractional constraint. And like the thermal field, the concentration of (GO) mixed nanofluid has a more significant impact than (MoS2) mixed

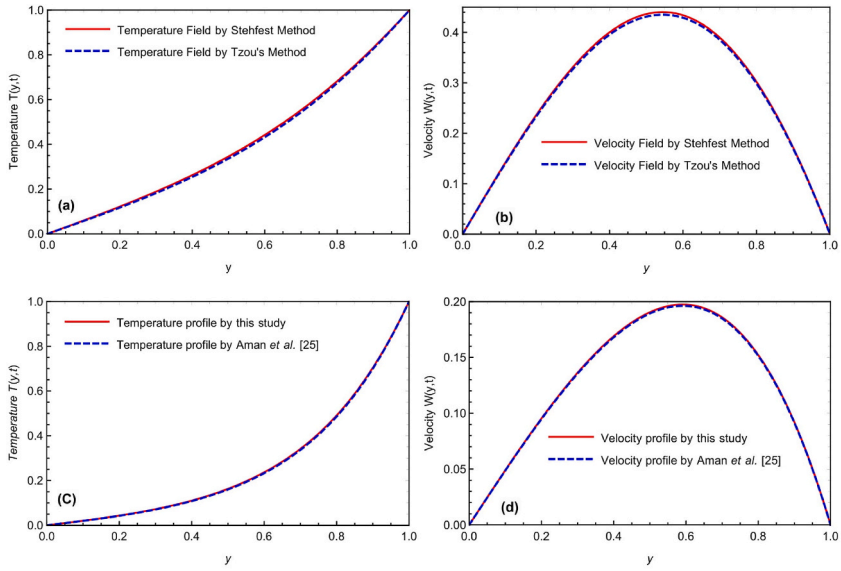

Fig. 6. Comparison of attained results with Aman et al. [25].

nanofluid for both fractional and Schmidt number cases. The velocity field dramatically benefits from the nanofluid density. The resulting hybrid nanofluids thicken substantially when base fluid and nanoparticles are joined, which lowers velocity and increases the temperature.

Fig. 3 (c, d) are strained to analyze the result of fractional constraints and radiation parameters on the momentum profile by fixing other constraints. The velocity field slows down due to enhancement in the fractional constraints due to the kernel of Prabhakar and the memory effect. This result is due to the fact that in this scenario, the thickness of the velocity boundary layer is less than that of the thermal boundary layer. The impact of N on the velocity profile is represented in Fig. 3(d). An increase in N values causes more heat to be transferred to the fluid, raising its temperature and improving the fractional nanofluid flow. Fig. 4(a) & (b) depict how K and *Pe* impact the momentum field. It is investigated whether velocity falls off at higher values of K. As K is raised, the drag forces weaken and the velocity decreases as a result. Physical explanations for this effect include the fact that as K is raised, drag forces become more vigorous, and as a result, velocity reduces for both K and *Pe* parameters. Physically, The viscous forces will be more assertive than the thermal forces as *Pe* values increase, which will decrease fluid velocity. The influence of heat and mass grashoof numbers are drawn in Fig. 4 (c, d) for the velocity field. A rise in buoyant forces resulting from an increase in *Gr* induces an increase in fluid velocity. Physically, the buoyancy forces improve as heat, mass grashoof numbers, and fluid velocity also rises.

Fig. 5(a) and (b) show how M affects the fluid velocity and how the magnetic field's tilt affects fluid velocity. The velocity decreases as M rises. Physically, at large values of M, this is true because M intensifies the Lorentz forces, which tend to slow velocity. Additionally, the applied magnetic field is strongest when it is orthogonal to the fluid flow. The effect of nanofluid Schmidt number and volume fraction φ are depicted in Fig. 5(c) & (d). This can be seen that the velocity profile indicates the decreasing behavior with the increment for both parameters. The physical explanation for this characteristic of velocity is that as the volume percentage of the nanoparticles increases, the fluid becomes stiffer, which causes a drop in the nanofluid velocity. The speed for the hybrid nanofluid reduces with rising values of φ. Physically, enhancing the volume fraction values increases the density and delays the porosity effect, due to which fluid moves more slowly. In the comparison of the velocities of several nanofluids is also shown. The graphic trend of the velocity profile reveals that $(GO-CMS)$ have a higher value as compared to (MoS_2-CMS) suspension. Physically, it is because $(GO-CMS)$ conducts substantial heat since it is effective despite being less dense. (GO) mixed suspension has the higher velocity among all the fluids considered here.

Table 5
The inspection of Sherwood number, Nusselt number, Skin friction at different time.

α	Nu for t = 0.5	Nu for t = 1.0	Sh for t = 0.5	Sh for t = 1.0	C_f for t = 0.5	C_f for t = 1.0
0.1	1.3413	1.3229	1.3875	1.4345	0.3106	0.3713
0.2	1.3621	1.3425	1.4128	1.4568	0.3291	0.4078
0.3	1.3874	1.3703	1.4463	1.4909	0.3580	0.4733
0.4	1.4131	1.4048	1.4813	1.5363	0.4027	0.5966
0.5	1.4362	1.4439	1.5132	1.5864	0.4667	0.8229
0.6	1.4550	1.4842	1.5359	1.6357	0.5413	1.2259
0.7	1.4687	1.5262	1.5589	1.6881	0.5889	1.7357
0.8	1.4773	1.5563	1.5714	1.7329	0.5334	1.9778
0.9	1.4814	1.5839	1.5778	1.7697	0.2748	1.0195

The inversion approaches of Stehfest and Tzou's algorithms, which are used to derive the numerical solutions of momentum and thermal fields, are drawn in Fig. 6(a) and (b) to demonstrate their viability. The temperature profile matching curves in Fig. 6(a) and the corresponding curves of velocity distribution in Fig. 6(b) show that the inversion algorithms are valid. Similarly, for the validity of attained results, the comparison of this study is associated with the accomplished results of Aman et al. [25]. The conclusion states that our results can be improved in terms of memory. Finally, the numerical comparison of all governed solutions attained by considered numerical techniques is analyzed in Tables 3 and 4 And the numerical analysis of Sherwood number, skin friction, and nusselt number at different time values is examined in Table 5. It is evident that the distributions of all (Nusselt number, Sherwood number, and Skin friction) rise as α rises. Additionally, the tables demonstrate that our approaches satisfy the mandated beginning and boundary requirements.

5. Conclusions

The free convective flow of a nanofluid flow that is unsteady and incompressible, combined with (GO) and (MoS_2) nanoparticles with (CMC) is explored. Using the most recent and improved characterization of a fractional derivative, the Prabhakar fractional derivative, a fractional model is constructed and then resolved using the LT. The effects of various parameters on the temperature, concentration, and momentum profile data are examined graphically and numerically. Following is a list of some notable findings from this work:

- As the Prabhakar fractional constraints rise, the temperature decreases and asymptotically rises over time.
- The velocity and concentration profiles also start to decline when the fractional constraints' values rise.
- Based on generalized assumptions, obtained solutions are expected for various values of fractional parameters. Better memory is achieved according to Fourier's law rather than artificial replacement.
- The two numerical techniques' solution curves line up, confirming our obtained results.
- By boosting the values of *Gr* and *Gm*, the velocity rises due to the buoyancy effect.
- In the comparison of nanofluids, *GO* based suspension has a more significant influence as compared to MoS_2 nanoparticles.
- The acquired solutions can be helpful for a thorough investigation of actual data and can be used as a tool to assess potential estimates of solutions when needed.
- By contrasting our acquired velocity solution with that of Aman et al. [25], it is further shown that the velocity profile results in graphical form are valid.

Author statement

Ali Raza: Conceptualization, Methodology, Writing - Original draft preparation, Data curation. **Ahmed M. Abed**: Conceptualization, Methodology, Writing - Original draft preparation. **M. Y Almusawa**: Methodology, Investigation, Resources, Writing - Reviewing and Editing. **Laila F. Seddek**: Investigation, Resources, Writing - Original draft preparation. **Ali Hasan Ali**: Software, Visualisation, Supervision, Writing - Reviewing and Editing.

Declaration of competing interest

The authors declare that they have no known competing financial interests or personal relationships that could have appeared to influence the work reported in this paper.

Data availability

Data will be made available on request.

Acknowledgment

This study is supported via funding from prince Sattam bin Abdulaziz University project number (PSAU/R1/1444).

References

[1] S.U. Choi, J.A. Eastman, Enhancing Thermal Conductivity of Fluids with Nanoparticles, Argonne National Lab.(ANL), Argonne, IL (United States), 1995.
[2] J. Buongiorno, Convective Transport in Nanofluids, 2006.
[3] M. Sheikholeslami, M. Gorji-Bandpy, D. Ganji, P. Rana, S. Soleimani, Magnetohydrodynamic free convection of Al2O3–water nanofluid considering Thermophoresis and Brownian motion effects, Comput. Fluid 94 (2014) 147–160.
[4] D. Domairry, M. Sheikholeslami, H.R. Ashorynejad, R.S.R. Gorla, M. Khani, Natural convection flow of a non-Newtonian nanofluid between two vertical flat plates, Proc. Inst. Mech. Eng. - Part N J. Nanoeng. Nanosyst. 225 (3) (2011) 115–122.
[5] Y.-Q. Song, et al., Significances of exponential heating and Darcy's law for second grade fluid flow over oscillating plate by using Atangana-Baleanu fractional derivatives, Case Stud. Therm. Eng. 27 (2021), 101266.
[6] M. Ahmad, M.I. Asjad, A. Akgül, D. Baleanu, Analytical Solutions for Free Convection Flow of Casson Nanofluid over an Infinite Vertical Plate, 2021.
[7] T. Gul, M. Bilal, W. Alghamdi, M.I. Asjad, T. Abdeljawad, Hybrid nanofluid flow within the conical gap between the cone and the surface of a rotating disk, Sci. Rep. 11 (1) (2021) 1–19.
[8] K. Rafique, M. Imran, M. Anwar, M. Misiran, A. Ahmadian, Energy and mass transport of Casson nanofluid flow over a slanted permeable inclined surface, J. Thermal Anl. Calorimet, 144 (6) (2021) 2031–2042.
[9] M.I. Asjad, M.D. Ikram, R. Ali, D. Baleanu, A.S. Alshomrani, New analytical solutions of heat transfer flow of clay-water base nanoparticles with the application of novel hybrid fractional derivative, Therm. Sci. 24 (Suppl. 1) (2020) 343–350.

[10] M.D. Ikram, M.I. Asjad, A. Akgül, D. Baleanu, Effects of hybrid nanofluid on novel fractional model of heat transfer flow between two parallel plates, Alex. Eng. J. 60 (4) (2021) 3593–3604.
[11] M.I. Khan, M. Waqas, T. Hayat, M.I. Khan, A. Alsaedi, Chemically reactive flow of upper-convected Maxwell fluid with Cattaneo–Christov heat flux model, J. Braz. Soc. Mech. Sci. Eng. 39 (2017) 4571–4578.
[12] Y.-Q. Song, et al., Solar energy aspects of gyrotactic mixed bioconvection flow of nanofluid past a vertical thin moving needle influenced by variable Prandtl number, Chaos, Solit. Fractals 151 (2021), 111244.
[13] M.I. Khan, T. Hayat, S. Qayyum, M.I. Khan, A. Alsaedi, Entropy generation (irreversibility) associated with flow and heat transport mechanism in Sisko nanomaterial, Phys. Lett. 382 (34) (2018) 2343–2353.
[14] A. Raza, et al., Thermal activity of conventional Casson nanoparticles with ramped temperature due to an infinite vertical plate via fractional derivative approach, Case Stud. Therm. Eng. 27 (2021), 101191.
[15] M.I. Khan, T. Hayat, S. Afzal, M.I. Khan, A. Alsaedi, Theoretical and numerical investigation of Carreau–Yasuda fluid flow subject to Soret and Dufour effects, Comput. Methods Progr. Biomed. 186 (2020), 105145.
[16] C. Fetecau, D. Vieru, C. Fetecau, Effect of side walls on the motion of a viscous fluid induced by an infinite plate that applies an oscillating shear stress to the fluid, Open Phys. 9 (3) (2011) 816–824.
[17] A. Sohail, D. Vieru, M. Imran, Influence of side walls on the oscillating motion of a Maxwell fluid over an infinite plate, Mechanics 19 (3) (2013) 269–276.
[18] S. Han, L. Zheng, X. Zhang, Slip effects on a generalized Burgers' fluid flow between two side walls with fractional derivative, J. Egyptian Mathemat. Soc. 24 (1) (2016) 130–137.
[19] J. Kang, Y. Liu, T. Xia, Unsteady flows of a generalized fractional Burgers' fluid between two side walls perpendicular to a plate, Adv. Mathemat. Phys. 2015 (2015).
[20] C. Fetecau, C. Fetecau, M. Kamran, D. Vieru, Exact solutions for the flow of a generalized Oldroyd-B fluid induced by a constantly accelerating plate between two side walls perpendicular to the plate, J. Non-Newtonian Fluid Mech. 156 (3) (2009) 189–201.
[21] D. Vieru, C. Fetecau, C. Fetecau, Flow of a viscoelastic fluid with the fractional Maxwell model between two side walls perpendicular to a plate, Appl. Math. Comput. 200 (1) (2008) 459–464.
[22] F. Wang, Z. Li, Y. Zhang, J. Guo, Fractional Derivative Modeling for Sediment Suspension in Ice-Covered Channels, Environmental Science and Pollution Research, 2022, pp. 1–13.
[23] Z.A. Khan, S.U. Haq, T.S. Khan, I. Khan, K.S. Nisar, Fractional Brinkman type fluid in channel under the effect of MHD with Caputo-Fabrizio fractional derivative, Alex. Eng. J. 59 (5) (2020) 2901–2910.
[24] S.R. Rao, G. Vidyasagar, G. Deekshitulu, Unsteady MHD free convection Casson fluid flow past an exponentially accelerated infinite vertical porous plate through porous medium in the presence of radiation absorption with heat generation/absorption, Mater. Today Proc. 42 (2021) 1608–1616.
[25] S. Aman, I. Khan, Z. Ismail, M.Z. Salleh, I. Tlili, A new Caputo time fractional model for heat transfer enhancement of water based graphene nanofluid: an application to solar energy, Results Phys. 9 (2018) 1352–1362.
[26] B.S. Goud, P.P. Kumar, B.S. Malga, Effect of heat source on an unsteady MHD free convection flow of Casson fluid past a vertical oscillating plate in porous medium using finite element analysis, Partial Different. Equat. Appl. Mathemat. 2 (2020), 100015.
[27] A. Ali, M. Umar, Z. Bukhari, Z. Abbas, Pulsating flow of a micropolar-Casson fluid through a constricted channel influenced by a magnetic field and Darcian porous medium: a numerical study, Results Phys. 19 (2020), 103544.
[28] P. Sunthrayuth, A. Alderremy, F. Ghani, A.M. Tchalla, S. Aly, Y. Elmasry, Unsteady MHD flow for fractional Casson channel fluid in a porous medium: an application of the Caputo-Fabrizio time-fractional derivative, J. Function Spaces 2022 (2022).
[29] F. Bräuer, E. Trautner, J. Hasslberger, P. Cifani, M. Klein, Turbulent Bubble-Laden channel flow of power-law fluids: a direct numerical simulation study, Fluid 6 (1) (2021) 40.
[30] Y. Zheng, H. Yang, H. Mazaheri, A. Aghaei, N. Mokhtari, M. Afrand, An investigation on the influence of the shape of the vortex generator on fluid flow and turbulent heat transfer of hybrid nanofluid in a channel, J. Thermal Anl. Calorimet, 143 (2) (2021) 1425–1438.
[31] C. Milici, G. Drăgănescu, J.T. Machado, Introduction to Fractional Differential Equations, Springer, 2018.
[32] N.A. Shah, X. Wang, H. Qi, S. Wang, A. Hajizadeh, Transient electro-osmotic slip flow of an oldroyd-B fluid with time-fractional Caputo-Fabrizio derivative, Journal of Applied and Computational Mechanics 5 (4) (2019) 779–790.
[33] N.N. Kumar, D. Sastry, S. Shaw, Irreversibility analysis of an unsteady micropolar CNT-blood nanofluid flow through a squeezing channel with activation energy-Application in drug delivery, Comput. Methods Progr. Biomed. 226 (2022), 107156.
[34] D. Sastry, N.N. Kumar, P.K. Kameswaran, S. Shaw, Unsteady 3D micropolar nanofluid flow through a squeezing channel: application to cardiovascular disorders, Indian J. Phys. (2022) 1–14.
[35] M. Nayak, G. Mahanta, M. Das, S. Shaw, Entropy analysis of a 3D nonlinear radiative hybrid nanofluid flow between two parallel stretching permeable sheets with slip velocities, Int. J. Ambient Energy 43 (1) (2022) 8710–8721.
[36] H.B. Yadeta, S. Shaw, Magnetic drug targeting during Casson blood flow in a microvessel: a Caputo fractional model, J. Magn. Magn Mater. (2023), 170363.
[37] J. Ndenda, J. Njagarah, S. Shaw, Role of immunotherapy in tumor-immune interaction: perspectives from fractional-order modelling and sensitivity analysis, Chaos, Solit. Fractals 148 (2021), 111036.
[38] S. Maiti, S. Shaw, G. Shit, Fractional order model of thermo-solutal and magnetic nanoparticles transport for drug delivery applications, Colloids Surf. B Biointerfaces 203 (2021), 111754.
[39] M. Caputo, M. Fabrizio, A new definition of fractional derivative without singular kernel, Prog. Fractional Differ. Appl. 1 (2) (2015) 73–85.
[40] A. Atangana, J.J. Nieto, Numerical solution for the model of RLC circuit via the fractional derivative without singular kernel, Adv. Mech. Eng. 7 (10) (2015), 1687814015613758.
[41] A. Atangana, On the new fractional derivative and application to nonlinear Fisher's reaction–diffusion equation, Appl. Math. Comput. 273 (2016) 948–956.
[42] M. Arif, F. Ali, N.A. Sheikh, I. Khan, K.S. Nisar, Fractional model of couple stress fluid for generalized Couette flow: a comparative analysis of Atangana–Baleanu and Caputo–Fabrizio fractional derivatives, IEEE Access 7 (2019) 88643–88655.
[43] S. Akhtar, Flows between two parallel plates of couple stress fluids with time-fractional Caputo and Caputo-Fabrizio derivatives, The European Phys. J. Plus 131 (11) (2016) 1–13.
[44] S. Ullah Khan, A. Raza, B. Prasannakumara, Y.D. Reddy, M.I. Khan, Inspecting heat transport phenomenon in the flow of non-Newtonian fluid in the presence of Newtonian heating and inclined slip: fractional derivative framework, Waves Random Complex Media (2023) 1–12.
[45] A. Raza, et al., Fractional order simulations for the thermal determination of graphene oxide (GO) and molybdenum disulphide (MoS2) nanoparticles with slip effects, Case Stud. Therm. Eng. 28 (2021), 101453.
[46] B. Guo, et al., Fractional-order simulations for heat and mass transfer analysis confined by elliptic inclined plate with slip effects: a comparative fractional analysis, Case Stud. Therm. Eng. 28 (2021), 101359.
[47] P. Mayeli, G.J. Sheard, Buoyancy-driven flows beyond the Boussinesq approximation: a brief review, Int. Commun. Heat Mass Tran. 125 (2021), 105316.
[48] Y.M. Chu, S. Bilal, M.R. Hajizadeh, Hybrid ferrofluid along with MWCNT for augmentation of thermal behavior of fluid during natural convection in a cavity, Math. Methods Appl. Sci. (2020).

[49] B. Fallah, S. Dinarvand, M. Eftekhari Yazdi, M.N. Rostami, I. Pop, MHD flow and heat transfer of SiC-TiO2/DO hybrid nanofluid due to a permeable spinning disk by a novel algorithm, Journal of Applied and Computational Mechanics 5 (5) (2019) 976–988.
[50] G.M. Mittag-Leffler, Sur la nouvelle fonction Eα (x), CR Acad. Sci. Paris 137 (2) (1903) 554–558.
[51] A. Wiman, Uber den fundamental Satz in der Theories der Funktionen Eα (z), Acta Math. 29 (1905) 191–201.
[52] T.R. Prabhakar, A Singular Integral Equation with a Generalized Mittag Leffler Function in the Kernel, 1971.
[53] A. Giusti, "Colombaro, I," Prabhakar-like fractional viscoelasticity, Commun. Nonlinear Sci. Numer. Simul. 56 (2018) 138.
[54] F. Polito, Z. Tomovski, Some properties of Prabhakar-type fractional calculus operators, arXiv preprint arXiv:1508.03224 (2015).
[55] H. Stehfest, Algorithm 368: numerical inversion of Laplace transforms [D5], Commun. ACM 13 (1) (1970) 47–49.